J|A|C|S ARTICLES

Published on Web 03/25/2010

Unexpected Binding Modes of Nitric Oxide Synthase Inhibitors Effective in the Prevention of a Cerebral Palsy Phenotype in an Animal Model

Silvia L Delker,[†] Haitao Ji,[‡] Huiying Li,[†] Joumana Jamal,[†] Jianguo Fang,[‡] Fengtian Xue,[‡] Richard B. Silverman,*[,‡] and Thomas L. Poulos*[,†]

Departments of Molecular Biology and Biochemistry, Pharmaceutical Sciences, and Chemistry, University of California, Irvine, California 92697-3900, and Department of Chemistry, Department of Biochemistry, Molecular Biology, and Cell Biology, Center for Molecular Innovation and Drug Discovery, and Chemistry of Life Processes Institute, Northwestern University, Evanston, Illinois 60208-3113

Received December 9, 2009; E-mail: poulos@uci.edu; agman@chem.northwestern.edu

Abstract: Selective inhibition of the neuronal isoform of nitric oxide synthase NOS (nNOS) has been shown to prevent brain injury and is important for the treatment of various neurodegenerative disorders. However, given the high active site conservation among all three NOS isoforms, the design of selective inhibitors is an extremely challenging problem. Here we present the structural basis for why novel and potent nNOS inhibitors exhibit the highest level of selectivity over eNOS reported so far (~3,800-fold). By using a combination of crystallography, computational methods, and site-directed mutagenesis, we found that inhibitor chirality and an unanticipated structural change of the target enzyme control both the orientation and selectivity of these novel nNOS inhibitors. A new hot spot generated as a result of enzyme elasticity provides important information for the future fragment-based design of selective NOS inhibitors.

Introduction

Nitric oxide (NO),[1] an essential signaling molecule involved in various physiological functions in humans,[2−4] is synthesized by a family of enzymes called nitric oxide synthase (NOS, EC 1.14.13.39).[5] NOS is active as a homodimer with each monomer containing a C-terminal reductase domain (with binding sites for NADPH, FAD, and FMN) and a N-terminal oxygenase domain containing the heme prosthetic group.[6] Both the substrate L-arginine and a redox cofactor, (6*R*)-5,6,7,8-tetrahydro-L-biopterin (H_4B), bind near the heme center in the oxygenase domain.[7,8] The over and under production of NO is responsible for a number of pathological conditions. The biosynthesis of NO by brain neuronal NOS (nNOS) is associated with stroke and chronic neurodegenerative diseases, such as Alzheimer's, Parkinson's, and Huntington's diseases.[9] As a result, drugs targeting nNOS should be of considerable therapeutic benefit.[10] However, humans also have two other NOS isoforms, one of which, endothelial NOS (eNOS), is essential for maintaining proper blood pressure.[11−13] Inhibition of eNOS results in hypertension and is an undesirable and even dangerous side effect of nonselective inhibitors targeted to nNOS. Isoform-selective drugs are essential if nNOS is to be a viable therapeutic target.[14] Herein lies the challenge, because the crystal structures of the catalytic domain of all three NOS isoforms show that the active sites are nearly identical,[7,8,15] making structure-based isoform-selective drug design a difficult and challenging problem.[16−19] Here we describe the synthesis, inhibitory constants, and crystal structures of a series of novel NOS

[†] University of California, Irvine.
[‡] Northwestern University.

(1) Pacher, P.; Beckman, J. S.; Liaudet, L. *Physiol. Rev.* **2007**, *87*, 315–424.
(2) Arnold, W. P.; Mittal, C. K.; Katsuki, S.; Murad, F. *Proc. Natal. Acad. Sci. U.S.A.* **1977**, *74*, 3203–3207.
(3) Furchgott, R. F.; Zawadzki, J. V. *Nature* **1980**, *288*, 373–376.
(4) Ignarro, L. J.; Adams, J. B.; Horwitz, P. M.; Wood, K. S. *J. Biol. Chem.* **1986**, *261*, 4997–5002.
(5) Alderton, W. K.; Cooper, C. E.; Knowles, R. G. *Biochem. J.* **2001**, *357*, 593–615.
(6) Roman, L. J.; Martásek, P.; Masters, B. S. *Chem. Rev.* **2002**, *102*, 1179–1190.
(7) Raman, C. S.; Li, H.; Martasek, P.; Kral, V.; Masters, B. S.; Poulos, T. L. *Cell* **1998**, *95*, 939–950.
(8) Crane, B. R.; Arvai, A. S.; Ghosh, D. K.; Wu, C.; Getzoff, E. D.; Stuehr, D. J.; Tainer, J. A. *Science* **1998**, *279*, 2121–2126.
(9) Calabrese, V.; Mancuso, C.; Calvani, M.; Rizzarelli, E.; Butterfield, D. A.; Stella, A. M. *Nat. Rev.* **2007**, *8*, 766–775.
(10) Hantraye, P.; Brouillet, E.; Ferrante, R.; Palfi, S.; Dolan, R.; Matthews, R. T.; Beal, M. F. *Nat. Med.* **1996**, *2*, 1017–1021.
(11) Huang, P. L.; Huang, Z.; Mashimo, H.; Bloch, K. D.; Moskowitz, M. A.; Bevan, J. A.; Fishman, M. C. *Nature* **1995**, *377*, 239–242.
(12) Braam, B.; Verhaar, M. C. *Curr. Pharm. Design* **2007**, *13*, 1727–1740.
(13) Endres, M.; Laufs, U.; Liao, J. K.; Moskowitz, M. A. *Trends Neurosci.* **2004**, *27*, 283–289.
(14) Vallance, P.; Leiper, J. *Nat. Rev. Drug Discovery* **2002**, *1*, 939–950.
(15) Li, H.; Shimizu, H.; Flinspach, M.; Jamal, J.; Yang, W.; Xian, M.; Cai, T.; Wen, E. Z.; Jia, Q.; Wang, P. G.; Poulos, T. L. *Biochemistry* **2002**, *41*, 13868–13875.
(16) Erdal, E. P.; Litzinger, E. A.; Seo, J.; Zhu, Y.; Ji, H.; Silverman, R. B. *Curr. Top. Med. Chem.* **2005**, *5*, 603–624.
(17) Garcin, E. D.; Bruns, C. M.; Lloyd, S. J.; Hosfield, D. J.; Tiso, M.; Gachhui, R.; Stuehr, D. J.; Tainer, J. A.; Getzoff, E. D. *J. Biol. Chem.* **2004**, *279*, 37918–37927.
(18) Salerno, L.; Sorrenti, V.; Di Giacomo, C.; Romeo, G.; Siracusa, M. A. *Curr. Pharm. Des.* **2002**, *8*, 177–200.
(19) Tafi, A.; Angeli, L.; Venturini, G.; Travagli, M.; Corelli, F.; Botta, M. *Curr. Med. Chem.* **2006**, *13*, 1929–1946.

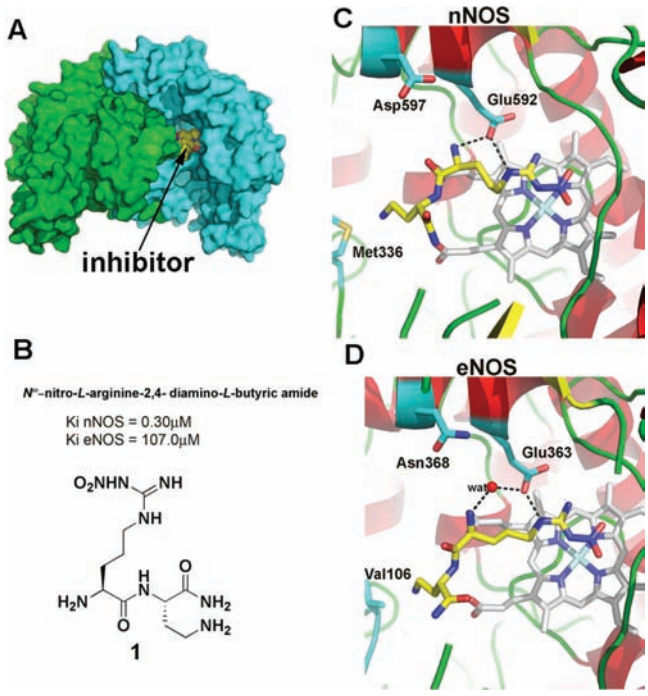

Figure 1. Inhibitor binding pocket in NOS (A) and the active site structure of nNOS (C) and eNOS (D) showing the different binding modes of the dipeptide inhibitor **1** (B) that exhibits about 1500-fold selectivity for nNOS over eNOS (Table 1).

inhibitors complexed to both nNOS and eNOS leading to the identification of unexpected binding modes as well as the identification of a flexible region of the NOS active site that can be exploited for structure-based drug design.

Results and Discussion

Structural Basis for Selectivity. Previous structure−activity relationship studies in our laboratories on a series of N^{ω}-nitro-L-arginine containing dipeptide inhibitors (**1** in Figure 1) have enabled us to identify a family of compounds that have high potency and selectivity for inhibition of nNOS over eNOS and iNOS.[20−26] The key structural features in the active site that are responsible for the lower K_i of these inhibitors to nNOS over eNOS have been identified by crystallographic and computational simulations. Most importantly, a single amino acid difference, Asp597 in nNOS and Asn368 in eNOS, has been identified as the major structural determinant for why these dipeptide inhibitors bind more tightly to nNOS than eNOS.[21] As shown in Figure 1, all NOS isoforms have a conserved Glu (Glu592 in nNOS and Glu363 in eNOS) in the active site pocket that helps to anchor the natural substrate, L-arginine, in place. The C_{α} end of the substrate is anchored in a second pocket that contains Asp597 in nNOS and Asn368 in eNOS. This pocket is only occupied with water molecules when dipeptide inhibitors bind. The flexible dipeptide inhibitors can adopt a curled conformation that allows the free α-amino group to interact with both the active site Glu592 and Asp597 in nNOS (Figure 1). Since eNOS has Asn368 at this position rather than Asp, these dipeptide inhibitors are electrostatically far less stable in the eNOS active site. As expected, the potency of these inhibitors can be dramatically increased in eNOS by replacing Asn368 with Asp, and K_i rises substantially in nNOS if Asp597 is replaced by Asn.[21]

Table 1. Inhibition of NOS Isozymes by **1**, **2**, and Four Enantiomerically Pure Isomers of **2**

	K_i (nM)			selectivity	
compound	nNOS	iNOS	eNOS	n/i	n/e
1	130	25 000	20 000	192	1538
(±)-**2**	14	4 060	28 000	290	2000
(3′*S*,4′*S*)-**2**	52.2	3 850	26 400	73.7	505
(3′*R*,4′*R*)-**2**	5.3	3 940	20 300	743	3830
(3′*R*,4′*S*)-**2**	18.9	16 100	57 100	852	3020
(3′*S*,4′*R*)-**2**	171.0	26 600	34 500	155	202

Inhibitor Design and K_i Measurements. Recently, we described a new strategy for the *de novo* design of nNOS-selective inhibitors called fragment hopping.[27] Using this novel approach together with what we learned from the dipeptide inhibitors described in the previous section, a series of compounds with a pyrrolidine methylaminopyridine scaffold (Figure 2) were designed and synthesized, which showed nanomolar nNOS inhibitory potency and more than 1000-fold nNOS selectivity.

These inhibitors were designed with the idea that the aminopyridine ring mimics the guanidinium group of L-arginine and anchors the compound in the active site by interacting with the active site glutamate. The rigid pyrrolidine ring is placed between the same conserved Glu and the selective residue nNOS Asp597/eNOS Asn368, which results in similar interactions observed by the α-amino group of dipeptide inhibitors bound to nNOS. Very recently, we showed that the racemic mixture of **2**, (±)-**2**, decreases NO levels and NOS activity in the brains of newborn rabbit kits, is nontoxic, and has no effect on the cardiovascular function of rabbit dams (indicating no impairment in eNOS function). Most importantly, (±)-**2** is very effective at protecting the rabbit fetuses from experimentally induced ischemic brain damage and preventing severe cerebral palsy symptoms in the newborn kits.[28] This is consistent with previous studies that have shown that nNOS knockout mice experience less neuronal damage as a result of experimentally induced ischemia.[29]

There are two chiral centers (3′ and 4′ carbons) in the structure of **2** (Figure 2). Our initial studies were carried out with the *cis*-racemic mixtures. Recognizing that chirality is critically important in drug design and that the enantiomers should eventually improve *in vivo* efficacy, we synthesized four enantiomerically pure isomers of **2** (see Supporting Information). The *in vitro* enzyme assay shows dramatic and unexpected

(20) Silverman, R. B. *Acc. Chem. Res.* **2009**, *42*, 439–451.
(21) Flinspach, M.; Li, H.; Jamal, J.; Yang, W.; Huang, H.; Hah, J.-M.; Gomez-Vidal, J. A.; Litzinger, E. A.; Silverman, R. B.; Poulos, T. L. *Nat. Struct. Mol. Biol.* **2004**, *11*, 54–59.
(22) Huang, H.; Martasek, P.; Roman, L. J.; Masters, B. S.; Silverman, R. B. *J. Med.* **1999**, *42*, 3147–3153.
(23) Seo, J.; Igarashi, J.; Li, H.; Martasek, P.; Roman, L. J.; Poulos, T. L.; Silverman, R. B. *J. Med. Chem.* **2007**, *50*, 2089–2099.
(24) Ji, H.; Gomez-Vidal, J. A.; Martasek, P.; Roman, L. J.; Silverman, R. B. *J. Med. Chem.* **2006**, *49*, 6254–6263.
(25) Gomez-Vidal, J. A.; Martasek, P.; Roman, L. J.; Silverman, R. B. *J. Med. Chem.* **2004**, 703–710.
(26) Hah, J. M.; Roman, L. J.; Martasek, P.; Silverman, R. B. *J. Med. Chem.* **2001**, *44*, 2667–2670.
(27) (a) Ji, H.; Stanton, B. Z.; Igarashi, J.; Li, H.; Martásek, P.; Roman, L. J.; Poulos, T. L.; Silverman, R. B. *J. Am. Chem. Soc.* **2008**, *130* (12), 3900–3914. (b) Ji, H.; Li, H.; Martasek, P.; Roman, L. J.; Poulos, T. L.; Silverman, R. B. *J. Med. Chem.* **2009**, *52*, 779–797.
(28) Ji, H.; Tan, S.; Igarashi, J.; Li, H.; Derrick, M.; Martasek, P.; Roman, L. J.; Vasquez-Vivar, J.; Poulos, T. L.; Silverman, R. B. *Ann. Neurol.* **2009**, *65*, 209–217.
(29) Huang, Z.; Huang, P. L.; Panahian, N.; Dalkara, T.; Fishman, M. C.; Moskowitz, M. A. *Science* **1994**, *265*, 1883–1885.

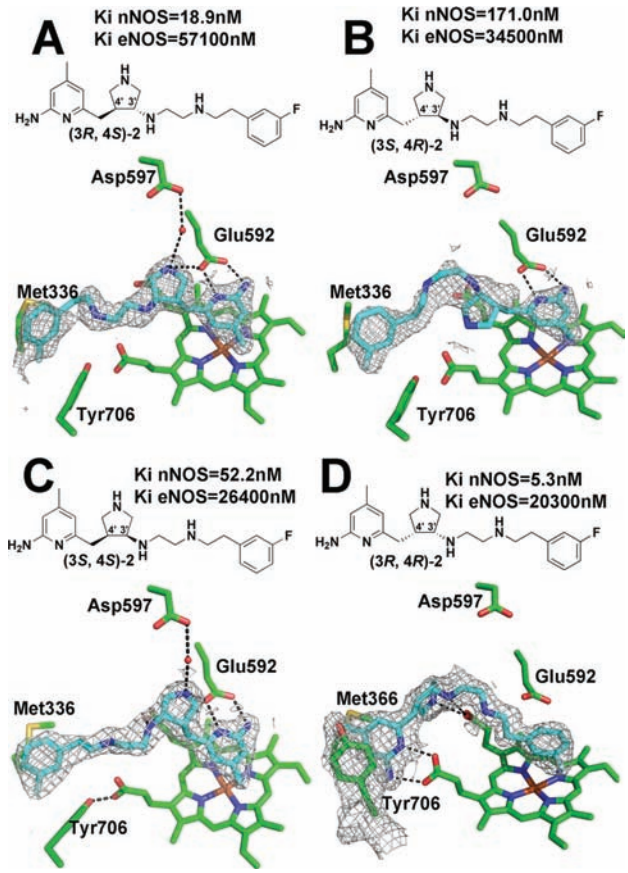

Figure 2. A series of $2F_o - F_c$ electron density maps contoured at 1.0σ for four various aminopyridine inhibitors bound to nNOS. Shown also their chemical formula and K_i values. Detailed refinement statistics are provided in Table S2 in Supporting Information. Briefly the resolution and R_{work}/R_{free} values for the 4 structures shown are (A) 1.93 Å, 0.18/0.21; (B) 1.98 Å, 0.18/0.21; (C) 1.95 Å, 0.19/0.22; and (D) 2.01 Å, 0.19/0.23.

results. The (3′*R*,4′*R*)-**2**, rather than (3′*S*,4′*S*)-**2**, is more potent and more selective for nNOS (Table 1). Its K_i is 5.3 nM, and the selectivities for nNOS over eNOS and over iNOS are more than 3,800-fold and 700-fold, respectively. With a K_i of ∼5 nM and ∼3,800-fold selectivity, this compound is, to the best of our knowledge, the most potent and dual-selective nNOS inhibitor reported to date. *Trans* (3′*R*,4′*S*)-**2** also is a very potent and selective inhibitor of nNOS with a K_i value of 19 nM for nNOS, and the nNOS selectivities over eNOS and iNOS are about 3,000-fold and 800-fold, respectively (Table 1).

Crystal Structures. Crystal structures of the *trans* (3′*R*,4′*S*)-isomer and the *trans* (3′*S*,4′*R*)-isomer show that these inhibitors bind as expected with the aminopyridine moiety interacting with active site Glu592 and the fluorophenyl group extending out of the substrate-binding site (Figure 2A,B). The reason why the (3′*S*,4′*R*)-isomer exhibits nNOS inhibitory activity lower than that of the (3′*R*,4′*S*)-isomer is readily understood on the basis of the crystal structures (Figure 2). In the structure with the (3′*R*,4′*S*)-isomer bound (Figure 2A), the pyrrolidine five-membered ring is positioned to H-bond with the active site Glu in nNOS. The ordered water bridges the pyrrolidine N atom and Asp597 in the (3′*R*,4′*S*) isomer-bound structure (Asn368 in eNOS, Figure S1 in Supporting Information). The positively charged nitrogen atom in the pyrrolidine ring interacts favorably with the side chain carboxylic group of Asp597 of nNOS (but not with the amide of Asn368, the corresponding residue in eNOS), which results in high nNOS selectivity over eNOS with

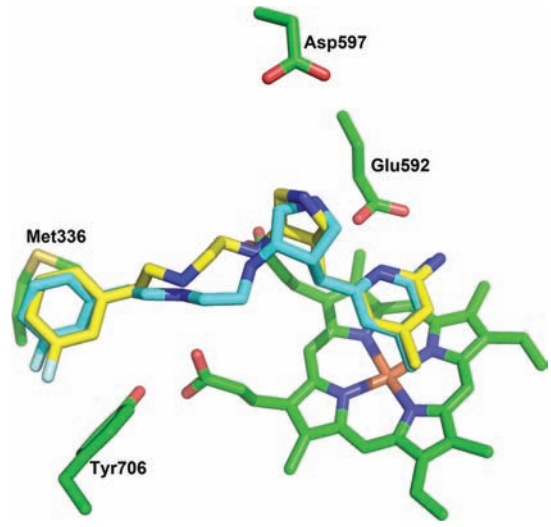

Figure 3. (3′*R*,4′*R*)-**2** (yellow) modeled in the same orientation as (3′*S*,4′*S*)-**2** (cyan) with an emphasis placed on minimizing steric clashes. It is not possible to model (3′*R*,4′*R*)-**2** in the (3′*S*,4′*S*)-**2** orientation and still maintain optimal inhibitor−protein H-bonds and minimal steric clashes.

this compound. Crystallographic analysis of (3′*S*,4′*R*)-**2** bound to nNOS (Figure 2B) is more ambiguous owing to the poorer quality of the electron density. Nonetheless, it is clear that this compound cannot be positioned to enable both the pyrrolidine and aminopyridine moieties to interact with the active site Glu. The (3′*R*,4′*S*)-inhibitor, therefore, forms better electrostatic interactions with neighboring protein groups (Figure 2A), which is the basis for the observed lower K_i of the (3′*R*,4′*S*)-inhibitor over the (3′*S*,4′*R*)-inhibitor. In addition, the 3-fluorophenyl ring is stabilized in a hydrophobic pocket defined by Met 336, Leu337, and Trp306 from the second monomer of nNOS. iNOS does not have this hydrophobic pocket. The residue corresponding to Leu337 of nNOS is Thr121 in human iNOS or Asn115 in murine iNOS. That is why the (3′*R*,4′*S*)-isomer exhibits more than 800-fold nNOS selectivity over iNOS.

As shown in Figure 2, the (3′*S*,4′*S*)-isomer binds to nNOS as expected, with the aminopyridine group interacting with active site Glu592, which is very similar to the binding mode of the *trans* (3′*R*,4′*S*)- and (3′*S*,4′*R*)-compounds. The (3′*R*,4′*R*)-isomer, however, exhibits a totally different and unexpected binding mode; it flips 180° from the expected orientation. The fluorophenyl group is positioned over the heme while the aminopyridine extends out of the active site where it forms a bifurcated salt bridge with heme propionate D. For this to occur, Tyr706 must swing out of the way to make room for the aminopyridine. The pyrrolidine N atom is placed right in the middle between heme propionate A (2.5 Å) and the carbonyl group of H_4B (2.8 Å) (Figure 2). Strong H-bonding and charge−charge interactions are expected between these groups.

In an attempt to understand why (3′*R*,4′*R*)-**2** flips relative to (3′*S*,4′*S*)-**2**, we modeled (3′*R*,4′*R*)-**2** in the normal orientation (Figure 3). Optimization of H-bonds between the inhibitor and protein would result in severe steric clashes. In the modeled orientation shown in Figure 3 the inhibitor would lose the H-bond from its pyrrolidine nitrogen and only form two H-bonds between the aminopyridine and Glu592. Indeed, it is not possible for the inhibitor to adopt a conformation that enables H-bonding interactions between the pyrrolidine N atom and protein. There is the possibility for a third H-bond with a heme propionate, but this would require movement of the aminopyridine, thereby

disrupting the stacking interaction with the heme and H-bonds with Glu592. Thus, it is not possible to maintain both optimal H-bonding and minimal steric clashes in this modeled orientation. The flipped orientation in the crystal structure provides better H-bonding opportunities with no steric problems.

A critical factor in controlling the flipped orientation of (3′*R*,4′*R*)-**2** is the ability of Tyr706 to swing out of the way and form $\pi-\pi$ interactions with the aminopyridine of the inhibitor. This is the first time that movement of this tyrosine residue has been observed in the NOS enzymes, and this generates a new hot spot for fragment-based inhibitor design with appropriate inducement.

Given that (3′*R*,4′*R*)-**2** has 3,800-fold lower K_i with nNOS than eNOS, we might anticipate yet another binding mode in eNOS, as in the case of **1**. However, the 2.0 Å structure of eNOS complexed to (3′*R*,4′*R*)-**2** and related inhibitors (Figure S1 in Supporting Information) show exactly the same binding mode and structural changes found in nNOS.

Basis for K_i Differences. There are two central questions to be addressed. First, why does (3′*R*,4′*R*)-**2** have 7- to 8-fold lower K_i with nNOS than (3′*S*,4′*S*)-**2**, and second, why is (3′*R*,4′*R*)-**2** more selective for nNOS over eNOS than is (3′*S*,4′*S*)-**2**? The answer to the first question centers on the different binding modes of the pyrrolidine moieties in these two inhibitors, and the distance-dependent electrostatic interaction is probably the key factor that determines the difference in K_i. The pK_a of the 2-amino-4, 6-dimethylpyridine moiety is about 7.1,[30] and it would be expected that the aminopyridine moiety of (3′*S*,4′*S*)-**2** is fully protonated when bound to NOS owing to direct contact with the conserved active site Glu592. However, the curled conformation of (3′*S*,4′*S*)-**2** places the pyrrolidine N atom about 4.1 Å from the aminopyridine. Since the protonated pyrrolidine N atom has a much higher pK_a, it should be fully protonated at neutral pH, and its close proximity to the aminopyridine will prevent full protonation of that moiety to avoid electrostatic repulsion. Moreover, the pyrrolidine N atom directly contacts the active site Glu, and therefore, charge neutrality is achieved by having only the pyrrolidine carry a positive charge and not the aminopyridine.

In sharp contrast, the aminopyridine and the pyrrolidine moieties of (3′*R*,4′*R*)-**2** adopt an extended conformation with the pyrrolidine N atom 4.9 Å from the aminopyridine. As a result of the extended conformation, the aminopyridine carries a full positive charge with little electrostatic repulsion from the positive charge on the pyrrolidine. Since the aminopyridine interacts with the heme D-ring propionate and the pyrrolidine with the heme A-ring propionate, charge neutrality is achieved by having each group in the inhibitor carry a positive charge. Furthermore, the coplanarity of the positively charged pyrrolidine N atom of (3′*R*,4′*R*)-**2** with heme propionate A leads to strong charge−charge interactions, while the pyrrolidine N atom of (3′*S*,4′*S*)-**2** is not at the center of the area of influence from Glu592, which results in relatively weak charge−charge interactions.

To test this hypothesis we have used the MM-PBSA computational approach to compute the free energy of binding of a series of (3′*S*,4′*S*)-**2** and (3′*R*,4′*R*)-**2**-like inhibitors for which we have crystal structures. In the first series of calculations we assume that the aminopyridine is fully protonated in all complexes while in the second we assume that the aminopyridine is half protonated in the (3′*S*,4′*S*)-**2** orientation but fully protonated in the (3′*R*,4′*R*)-**2** orientation. As shown in Figure S2 in Supporting Information, the calculated free energies agree much better with the experimental free energies if we assume that the aminopyridine is only partially charged in the (3′*S*,4′*S*)-**2** orientation. It thus appears that the reason (3′*R*,4′*R*)-**2** is a better inhibitor than (3′*S*,4′*S*)-**2** is because of stronger electrostatic interactions between the inhibitor and the protein, including the heme.

Table 2. Inhibition of NOS Isozymes and Mutants by (3′*S*,4′*S*)-**2** and (3′*R*,4′*R*)-**2**

	K_i (μM)	
enzyme	(3′*S*,4′*S*)-**2**	(3′*R*,4′*R*)-**2**
nNOS wild type	0.0522	0.0053
nNOS D597N	1.19	0.29
nNOS D597N/M336V	1.19	0.18
nNOS D597N/M336V/Y706A	2.18	1.29
eNOS wild type	26.4	20.3
eNOS Y477A	46.0	35.2
eNOS N368D	2.29	0.50
eNOS N368D/V106M	1.41	0.23

The 700-fold nNOS selectivity of (3′*R*,4′*R*)-**2** over iNOS is primarily from the 4-methyl group of the 2-aminopyridine moiety, which can be stabilized in a hydrophobic pocket defined by Met336, Leu337, and Trp306 from the second monomer of nNOS. The therapeutically more interesting and more challenging question, however, is how to explain why the flipped orientation of (3′*R*,4′*R*)-**2** leads to greater selectivity for nNOS over eNOS despite the fact that the crystal structures show identical binding modes in both eNOS and nNOS. In previous studies we have shown that Asp597 (Asn in eNOS) and to a lesser extent Met336 (Val in eNOS) are largely responsible for the higher affinity of dipeptide inhibitors to nNOS.[21] Met336 provides more extensive interactions with the aminopyridine that extends out of the substrate-binding site pocket in nNOS, whereas Asp597 might provide greater electrostatic stabilization.

As shown in Table 2, the D597N/M336V double nNOS mutant exhibits a K_i for (3′*R*,4′*R*)-**2** of 0.18 μM compared to 5.3 nM for wild type nNOS, and 0.23 μM for the eNOS double mutant compared to 20.3 μM for wild type eNOS. While the Asp/Asn and Met/Val differences contribute to selectivity, there clearly must be other factors involved. The one additional subtle difference we have consistently noted is that the interaction between Tyr706 (Tyr477 in eNOS) and the aminopyridine is more extensive in nNOS than in eNOS (Figure S1 in Suporting Information). This could provide better nonbonded contacts as well as better desolvation of the inhibitor in nNOS. We therefore made a triple nNOS mutant, D597N/M336V/Y706A, and compared the K_i values to that of the single Y477A eNOS mutant. The D597N/M336V/Y706A triple nNOS mutant exhibits a K_i with (3′*R*,4′*R*)-**2** of 1.29 μM compared to 5.3 nM for wild type nNOS and 20.3 μM for wild type eNOS.

The single Y477A eNOS mutant exhibits a K_i with (3′*R*,4′*R*)-**2** of 35.2 μM (see Table 2). Tyr477 contributes little to no binding in eNOS but does contribute substantially in nNOS. Therefore, the reason (3′*R*,4′*R*)-**2** in the flipped orientation is more selective for nNOS than other inhibitors is a combination of better electrostatic interactions between the inhibitor and the active site in nNOS and the more favorable nonbonded contacts formed between Tyr706 and the inhibitor bound to nNOS.

In summary, we have designed, prepared, and solved crystal structures of a series of very potent and highly selective nNOS inhibitors, which we have previously demonstrated exhibit

(30) Paudler, W. W.; Blewitt, H. L. *J. Org. Chem.* **1966**, *31*, 1295–1298.

remarkable protection of newborn rabbit kits against the phenotype of cerebral palsy experimentally induced by hypoxia-ischemia. By using a combination of crystallography, computational biochemistry, and site-directed mutagenesis, we found that inhibitor chirality and the unexpected structural elasticity of NOS cause the inhibitor to adopt a novel binding mode and generate a new hot spot for ligand binding. These findings now can be utilized to design even more selective and potent drug-like NOS inhibitors.

Experimental Section

Crystallography. For crystallization the heme domain of isozymes nNOS and eNOS were isolated as described previously.[15,21,31] Cocrystallization of nNOS or eNOS crystals with inhibitors was abandoned due to the disturbance by inhibitors to the growth conditions. Instead, 10 mM histidine or 2 mM imidazole was added to the nNOS or eNOS samples, respectively, to occupy the heme active site before crystallization setup. Crystals grew within 24−48 h at 4 °C (eNos, 20 mg/mL or nNOS, 7−9 mg/mL) using the sitting drop vapor diffusion method as described.[15,21,31] Crystals were passed stepwise through a series of cryoprotectant solutions[15,21,31] before soaking with 10 mM inhibitors at 4 °C for 4−6 h and then were flash cooled with liquid nitrogen.

Both isoforms crystallized in space group $P2_12_12_1$ with typical unit cell dimensions $a = 52.0$, $b = 112.4$, $c = 164.6$ Å for nNOS and $a = 58.6$, $b = 107.1$, $c = 157.7$ Å for eNOS. The X-ray diffraction data were collected under a liquid nitrogen stream (100K) with CCD detectors either at Advanced Light Source (ALS, Berkeley, CA) or Stanford Synchrotron Radiation Lightsource (SSRL, Menlo Park, CA). Raw data were processed with HKL2000.[32] The binding of inhibitor was detected by difference Fourier synthesis. The inhibitor was modeled in using O[33] and refined with CNS[34] and then with REFMAC[35] to include the TLS protocol.[36] Water molecules were added automatically and inspected visually in COOT.[37] The refined structures were validated before deposition to the PDB. The data collection and refinement statistics are summarized in Table S1 in Supporting Information.

Computational Methods. The MM-PBSA method as implemented in Amber 9.0 was used to compute binding free energy.[38] In this method the total free energy of the NOS-inhibitor complex is taken as the sum of the following energy terms:

$$G = E_{MM} + G_{solv} + G_{np} - TS_{solute}$$

where E_{MM} = the total molecular mechanics energy computed with the Sander module in Amber 9.0, G_{solv} is the solvation free energy estimated from the Poisson−Boltzmann equation, G_{np} is the nonpolar solvation energy estimated from the solvent accessible surface area, and TS_{solute} is the solute entropy. From a single energy minimized structure the free energy is computed for the NOS-inhibitor complex, NOS alone with the inhibitor removed, and the inhibitor alone. The overall free energy of binding is computed from the following equation:

$$\Delta G_{bind} = (G_{complex} - G_{receptor} - G_{inhibitor})$$

As others have done the solute entropy is ignored.[39] Given that the inhibitors used for these calculations are structurally very similar with a similar number of rotatable bonds, ignoring inhibitor entropy introduces little error in comparing relative calculated and experimental free energies but does, of course, preclude the calculation of absolute free energies.

Inhibitor parameters and charges are assigned using the GAFF force field[40] and AM1-BCC charge scheme[41,42] as implemented in the Antechamber module in Amber 9.0. Heme parameters developed for cytochrome P450 were provided by Dr. Dan Harris.[43] It is necessary to carefully check the Antechamber output to make sure the correct atom types have been assigned. For some inhibitors it has been necessary to increase the force constant on improper torsion angles from 1.1 to 10.1 kcal/Å in order to maintain planarity of the aminopyridine groups. To prepare the models for energetic calculations all crystallographic waters are removed and TIP3 waters added back within 30 Å of the inhibitor. The resulting solvated structure is first energy minimized using the steepest descent method for 1,000 cycles with the inhibitor and heme heavy atoms restrained to the starting crystallographic positions. The restraints are relaxed to 10.0 kcal/Å^2 for the inhibitor and heme followed by another 1,000 cycles of refinement. In the last step the restraints for the heme and inhibitor were relaxed to 1.0 kcal/Å^2 followed by 1,000 cycles of minimization.

Enzymes, Assays, and K_i. All of the NOS isozymes used were recombinant enzymes overexpressed in *E. coli*. The murine macrophage iNOS was expressed and isolated according to the procedure of Hevel et al.[44] The constitutive full-length isozymes nNOS and eNOS were isolated as described previously,[21,31] with the exception that buffer containing 15 mM $NADP^+$ was used to elute wild type eNOS and eNOS N368D mutant from the 2′,5′-ADP sepharose column (GE Healthcare). Nitric oxide formation from NOS was monitored by the hemoglobin capture assay as described with some modifications.[45] The Hb assay mixture contained L-arginine (10 μM), NADPH (0.1 mM), tetrahydrobiopterin (10 μM), dithiothreitol (100 μM), Hb (0.1 mg/mL), CaM (10 μg/mL), $CaCl_2$ (0.1 mM), and different amounts of inhibitors. The final volume was adjusted to 600 μL with 100 mM Hepes buffer, pH 7.4. The enzymatic reaction was initiated by addition of enzyme, and the rate of NO production was monitored by the change of absorbance at 401 nm in the initial 60 s on a Perkin-Elmer Lambda 10 UV/vis spectrophotometer. The IC_{50} values were obtained from the dose-dependent inhibition curves. The inhibition constant (K_i) was calculated on the basis of the following equation:[46] $K_i = IC_{50}/(1 + [\text{substrate}]/K_m)$, where the K_m values of WT enzymes were as reported[47] and the K_m values of the mutant enzymes were experimentally determined by the Hb assay (Supplementary Table 2). All assays were performed at room temperature. The selectivity of an inhibitor was defined as the ratio of the respective K_i values.

(31) Li, H.; Flinspach, M. L.; Igarashi, J.; Jamal, J.; Yang, W.; Gomez-Vidal, J. A.; Litzinger, E. A.; Huang, H.; Erdal, E. P.; Silverman, R. B.; Poulos, T. L. *Biochemistry* **2005**, *44*, 15222–15229.
(32) Otwinowski, Z.; Minor, W. *Methods Enzymol.* **1997**, *276*, 307–326.
(33) Jones, T. A.; Zou, J.-Y.; Cowan, S. W.; Kjeldgaarrd, M. *Acta Crystallogr.* **1991**, *A47*, 110–119.
(34) Brunger, A. T.; Adams, P. D.; Clore, G. M.; DeLano, W. L.; Gros, P.; Grosse-Kunstleve, R. W.; Jiang, J. S.; Kuszewski, J.; Nilges, M.; Pannu, N. S.; Read, R. J.; Rice, L. M.; Simonson, T.; Warren, G. L. *Acta Crystallogr. D* **1998**, *54*, 905–921.
(35) Murshudov, G. N.; Vagin, A. A.; Dodson, E. J. *Acta Crystallogr.* **1997**, *D53*, 240–255.
(36) Winn, M. D.; Murshudov, G. N.; Papiz, M. Z. *Methods Enzymol.* **2003**, *374*, 300–321.
(37) Emsley, P.; Cowtan, K. *Acta Crystallogr.* **2004**, *D60*, 2126–2132.
(38) Massova, I.; Kollman, P. A. *J. Am. Chem. Soc.* **1999**, 8133–8143.
(39) Brown, S. P.; Muchmore, S. W. *J. Chem. Inf. Model* **2006**, *46*, 999–1005.
(40) Wang, J.; Wolf, R. M.; Caldwell, J. W.; Kollman, P. A.; Case, D. *J. Am. Chem. Soc.* **2004**, *25*, 1157–1174.
(41) Jakalian, A.; Bush, B. L.; Jack, D. B.; Bayly, C. I. *J. Comput. Chem.* **2000**, *21*, 132–146.
(42) Jakalian, A.; Jack, D. B.; Bayly, C. I. *J. Comput. Chem.* **2002**, *23*, 1623–1641.
(43) Harris, D. L.; Park, J. Y.; Gruenke, L.; Waskell, L. *Proteins* **2004**, *15*, 895–914.
(44) Hevel, J. M.; White, K. A.; Marletta, M. A. *J. Biol. Chem.* **1991**, *266*, 22789–22791.
(45) Hevel, J. M.; Marletta, M. A. *Methods Enzymol.* **1994**, *233*, 250–258.
(46) Segel, I. H. *Enzyme Kinetics*; John Wiley and Sons: New York, 1975.
(47) Hah, J. M.; Martasek, P.; Roman, L. J.; Silverman, R. B. *J. Med. Chem.* **2003**, *46*, 1661–1669.

Chemical Synthesis. The synthetic route, experimental details, and ^{1}H NMR and ^{13}C NMR spectra for the final products are provided in Supporting Information.

Acknowledgment. The authors are grateful for financial support from NIH with grants GM57353 (T.L.P) and GM49725 (R.B.S.). We thank the beamline staff at ALS and SSRL for their excellent support during the data collections.

Supporting Information Available: Details of chemical synthesis, a table of crystallographic statistics, and a description of 11 additional NOS-inhibitor complexes. This material is available free of charge via the Internet at http://pubs.acs.org.

JA910228A